International Journal of Pharmaceutics 416 (2011) 384–393

Contents lists available at ScienceDirect

International Journal of Pharmaceutics

journal homepage: www.elsevier.com/locate/ijpharm

Pharmaceutical Nanotechnology

A novel fluorescent probe for more effective monitoring of nanosized drug delivery systems within the cells

Karmen Teskač Plajnšek[a], Stane Pajk[a], Biljana Govedarica[a], Slavko Pečar[a,b], Stane Srčič[a], Julijana Kristl[a,*]

[a] University of Ljubljana, Faculty of Pharmacy, Aškerčeva 7, 1000 Ljubljana, Slovenia
[b] Institut Jožef Stefan, Jamova 39, 1000 Ljubljana, Slovenia

ARTICLE INFO

Article history:
Received 10 May 2011
Received in revised form 21 June 2011
Accepted 24 June 2011
Available online 1 July 2011

Keywords:
Nanoparticle, Fluorescent lipid probe
Coumarin derivative
Nanoparticles' trafficking
Cellular uptake
Intracellular location
Drug delivery

ABSTRACT

To improve visualization of nanoparticles within the cells' compartments, we synthesized a coumarin based fluorescent derivative, tetradecyl diethylamino coumarin amid, 14-DACA. In this compound the coumarin chromophore is linked with a tetradecyl alkyl chain that contributes to lipophilicity and slightly amphiphilic character of this probe. 14-DACA exhibits good biocompatibility, its solubility and emission spectrum are not sensitive to changes in pH value. Solid lipid nanoparticles (SLN) labeled with 14-DACA (SLN-D) and frequently used 6-coumarin (SLN-C) were utilized to evaluate probes' properties in the trafficking and intracellular localization of nanoparticles. SLN-D were seen as distinct blue dots in the cellular environment in contrast to SLN-C which were hardly to recognize due to the self-quenching of 6-coumarin, its leakage and distribution in intracellular compartments. Spectra of 14-DACA indicated the possibility of spectral resolution from both green and red fluorophores allowing clear multicolor imaging of organelles in both fixed and living cells. The results showed valuableness of new probe for trafficking of the drug nanocarriers intracellularly in a kinetic and sensitive manner. Such studies are of great importance in investigations aimed to clarify subcellular targeted drug delivery, controlled release and even to identify toxicological changes.

1. Introduction

Nanoparticles (NPs) are a rapidly growing class of colloidal carrier systems, particularly interesting in terms of their pharmaceutical applications. They demonstrate numerous advantages, such as the possibility of controlled drug targeting and release, high drug payload, increased stability of loaded drug, incorporation of lipophilic and hydrophilic drugs, low to non-existent biotoxicity of the carrier, etc. (Müller et al., 2000). Various physical methods can be used to characterize NPs, but evidently, techniques for imaging and monitoring, especially in biological systems, are of primary importance.

Fluorescence spectroscopy is a relatively simple technique for examining NPs in biological systems (White and Errington, 2005). The rapid development of fluorescent dyes and probes enables new opportunities for applying fluorescence spectroscopy in all branches of biomedical sciences, from visualizing cellular components and machinery up to the trafficking of nanoparticulate drug delivery systems in the cellular environment (Watson et al., 2005). Currently available fluorescent probe for staining particular cellular components are very well adjusted for specific and selective staining. In contrast, there is a lack of corresponding fluorescent probes for selective labeling of nanosized drug delivery systems (Wu et al., 2008), and is strongly dependent on adequate fluorescent probes (Torchilin, 2005). Cell structures and nanosized particles can be distinguished by their labeling with different fluorescent probes that have distinct excitation and emission wavelengths. To study structural and dynamic relation of NPs to other cellular organelles, multicolor fluorescence imaging is a standard approach. Selected fluorescent probes have to provide bright fluorescence profiles and should be sufficiently photostable (Sharma et al., 2006). Fluorescent probes also have to provide good visualization of NPs within cells in which particular cell structures are already labeled. Finally, to monitor solid lipid nanoparticles (SLN), such probes should be permanently attached to the NPs during the time of experiment, and its exchange with other cellular structure should be negligible.

In general, labeling of pharmaceutical colloidal carriers (e.g. liposomes, polymeric NPs, SLN, polymeric micelles) is related to the usage of commercially available fluorescent probes, such as are simple derivatives of coumarin ($\lambda_{ex}/\lambda_{em} \sim 370/450$ nm), cyanine ($\lambda_{ex}/\lambda_{em} \sim 550/570$ nm or higher), fluorescein ($\lambda_{ex}/\lambda_{em} \sim 490/520$ nm) and rhodamine ($\lambda_{ex}/\lambda_{em} \sim 540/570$ nm) (Sharma

* Corresponding author. Tel.: +386 1 4769500; fax: +386 1 4258031.
E-mail address: julijana.kristl@ffa.uni-lj.si (J. Kristl).

0378-5173/$ – see front matter © 2011 Elsevier B.V. All rights reserved.
doi:10.1016/j.ijpharm.2011.06.046

et al., 2006). In particular, the 3-carboxylic acid derivative of 7-diethylaminocoumarin and AMCA (7-amino-4-methyl coumarin-3-acetic acid), possess carboxylic groups which are suitable for making various coumarin derivatives or for coupling to proteins and other molecules. Those derivatives have pronounced stability to photobleaching, retaining their complete fluorescence over 3 times longer than fluorescein-based probes. Moreover, they possess intense fluorescence properties depending on attached group and next, they are mostly sensitive to the environmental changes influencing on alterations in solubility and emission spectrum intensity (Maier et al., 2002). For instance, the main disadvantage of labeling with rhodamine is its pH-dependent solubility (Panyam et al., 2003). When NPs, loaded with rhodamine, were endocytosed into the endo-lysosomes, the red dye was released, which could lead to an inaccurate intracellular pattern. On the other hand, 6-coumarin-loaded NPs are useful for short term *in vivo* pharmacokinetics and tissue distribution studies (Cu and Saltzman, 2009; Hironaka et al., 2009) but the usefulness of 6-coumarin in long term studies has not been determined yet (Gonçalves, 2009; Panyam et al., 2003).

In a series of recent studies, liposomes and SLN, both loaded with the chemopreventive resveratrol, were stained with 6-coumarin to visualize their cellular uptake and intracellular fate. Those nanosized delivery particles showed rapid internalization, however, the obtained results were unclear due to the rapid release of 6-coumarin from SLN in the cell interior (Caddeo et al., 2008; Kristl et al., 2009; Teskac and Kristl, 2010). Moreover, numerous researches were unable to ascertain precise intracellular localization of nanosized drug delivery systems, such as SLN (Miglietta et al., 2000), cyclodextrins (Cavalli et al., 2009), polymeric NPs (Cu and Saltzman, 2009; Harush-Frenkel et al., 2007; Panyam and Labhasetwar, 2003; Trapani et al., 2009) in cell cultures using 6-coumarin, because of its fast distribution with the surrounding environment and structures.

Despite many fluorescent derivatives used for imaging purposes also a set of structurally diverse fluorescent conjugates, mostly with rhodamine, were synthesized to study a wide range of biological events *in vitro* and *in vivo* (Hearnden et al., 2009; Gillmeister et al., 2011; Biswas et al., 2011). To clarify some of the issues regarding translocation of carriers from the endosomal compartment into the cellular cytosol even dual fluorescent labeling was used (Gillmeister et al., 2011).

To overcome these obstacles and complicated procedures we have designed and synthesized a new coumarin-based fluorescent probe, tetradecyl diethylamino coumarin amid, 14-DACA, for tightly anchoring to SLN, with minimal overlaying of fluorescent spectra of stained NPs and cell compartments. Thus, the main goal was to evaluate safeness and labeling properties of a synthesized fluorescent probe, 14-DACA throught *in situ* cell monitoring using fluorescent microscopy. Other complementary techniques provide additional results regarding physicochemical properties in order to get clear impression of main advantages of utilized agent among commercially available probes. In fact, we present new fluorescent probe enabling the possibility of spectral resolution from green and red fluorescence and multicolor imaging in both fixed and living cells, what to our knowledge, have so far been out of reach.

2. Experimental

2.1. Materials

Glyceryl behenate (Compritol® 888 ATO) was obtained from Gattefosse (France), hydrogenated soya bean lecithin (Phospholipon 90H) from Natterman (Germany) and a block copolymer of polyethylene and polypropylene glycol, Lutrol F68 (Poloxamer 188) from BASF AG (Ludwigshaften, Germany). 6-Coumarin was obtained from Sigma (Germany). Water was purified by reverse osmosis. Cell culture reagents were obtained from Sigma (Germany), unless otherwise indicated. All other chemicals (Sigma–Aldrich and Acros) were of analytical grade and were used without further purification.

2.2. Synthesis and physicochemical evaluation of 7-(diethylamino)-2-oxo-N-tetradecyl-2H-chromene-3-carboxamide (14-DACA)

14-DACA, as a derivative of commercially available 6-cumarin, was designed and synthesized according to standard coupling. Schematic presentation of the last step of 14-DACA synthesis is presented in Fig. 1. Compound 1 (7-diethylaminocoumarin-3-carboxylic acid) (1, 400 mg, 1.53 mmol) and N-methylmorpholine (NMM, 421 μL, 2.5 equiv, 3.82 mmol) were dissolved in dry dichloromethane (DCM, 5 mL) and the solution cooled to 0 °C on ice (Pajk and Pečar, 2009; Robert et al., 2008). *O*-(benzotriazol-1-yl)-*N*,*N*,*N*′,*N*′-tetramethyluronium tetrafluoroborate (TBTU, 590 mg, 1.2 equiv., 1.84 mmol) was added to the reaction mixture, followed by tetradecyl amine (490 mg, 1.5 equiv., 2.30 mmol) after 20 min. The reaction mixture was allowed to reach room temperature and stirring was continued for 2 h. The solvent was evaporated under reduced pressure and the residue dissolved in ethyl acetate (40 mL), washed with 0.1 M HCl (30 mL), saturated aqueous solution of $NaHCO_3$ (30 mL), brine (30 mL) and dried with Na_2SO_4. The solvent was evaporated under reduced pressure and the crude product purified by flash chromatography (ethyl acetate/hexane, 1:10–2:3) to give 14-DACA (570 mg, 1.25 mmol, 81%) as a yellow solid.

The obtained compound 14-DACA was analyzed by analytical TLC on Merck silica gel (60 F_{254}) plates (0.25 mm), visualized with ultraviolet light and stained with 20% sulfuric acid in ethanol. Flash chromatography was performed on an Isolera One flash purification system from Biotage using KP-Sil SNAP cartridges. ^1H and ^{13}C NMR spectra were recorded on a Brucker AVANCE DPX300 spectrometer in $CDCl_3$ solution with TMS as internal standard. Microanalysis was performed on a Perkin-Elmer C, H, N analyzer 240 °C. Mass spectra were recorded using a VG-Analytical Q-TOF Premier mass spectrometer. Absorbance and fluorescence spectra of fluorescent probes were scanned by automated plate reader (Tecan, Mannedorf/Zürich, Switzerland).

Physicochemical characteristics of 14-DACA are: Mp: 79–81 °C. IR (KBr, cm^{-1}): 3448, 3331, 2921, 2850, 2360, 1696, 1618, 1587, 1533, 1417, 1355, 1134, 794. ^1H NMR ($CDCl_3$, 300 MHz): δ (ppm) 8.77 (t, 1H, J = 5.4 Hz, NH), 8.70 (s, 1H, CH–Ar), 7.42 (d, 1H, J = 9.0 Hz, CH–Ar), 6.63 (dd, 1H, J_1 = 9.0 J_2 = 2.4 Hz, CH–Ar), 6.49 (d, 1H, J = 2.4 Hz, CH–Ar), 3.48–3.39 (m, 6H, 2 × CH_2–N, CH_2–NH), 1.65–1.56 (m, 2H, CH_2–CH_2NH), 1.40–1.15 (m, 28H, 2 × CH_3–CH_2N, 11 × CH_2), 0.87 (t, 3H, J = 6.9 Hz, CH_3–$(CH_2)_{13}$). ^{13}C NMR ($CDCl_3$, 75 MHz): δ (ppm) 162.79, 162.58, 157.43, 152.28, 147.73, 130.89, 110.47, 109.74, 108.27, 96.43, 44.92, 39.56, 31.97, 29.56, 29.52, 29.48, 29.46, 29.42, 29.22, 26.96, 22.56, 13.98, 12.31. HRMS (ESI), m/z calcd for $C_{28}H_{45}N_2O_3$ 457.3430 $(M+H)^+$, found 457.3441. Microanalysis calculated for $C_{28}H_{44}N_2O_3 \cdot 0.25\,C_6H_{14}$ (%): C 74.09, H 10.01, N 5.86; found C 74.11, H 10.38, N 6.14.

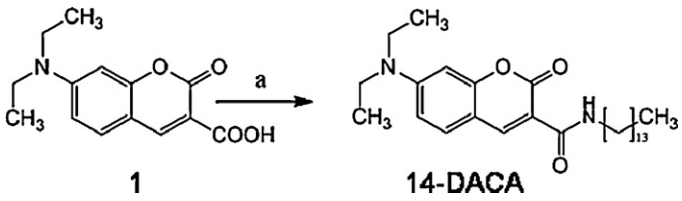

Fig. 1. Synthesis of 14-DACA; reaction conditions (a): tetradecylamine, TBTU, NMM, DCM, 0 °C, 2 h.

2.3. Preparation of SLN and labeling procedure

SLN were prepared by the melt-emulsification process, described elsewhere (Ahlin et al., 1998). The lipid Compritol 888ATO (20 mg; 0.2%, w/w) and Phospholipon 90H (15 mg; 0.15%, w/w) were melted at approximately 10 °C above the melting point, then half (5 g) of a hot aqueous solution of steric stabilizer Lutrol 188 (10 mg, 0.1%, w/w) was added and dispersed for 10 min at 15,000 rpm stirring with a rotor-stator homogenizer (Omni International, Gainesville, USA) to yield a dispersion of small liquid droplets in water. This dispersion was further diluted with the remaining steric stabilizer Lutrol 188, fast cooling of lipids and formation of NPs.

SLN were labeled with 14-DACA (SLN-D) and 6-coumarin (SLN-C). In both cases the ethanol solution of 14-DACA or 6-coumarin (approx. 1 mg; 0.01%, w/w; 1 mL) was added to the lipid phase before melting. Further steps were as those as used for the unlabeled NPs.

2.4. Physical characterization of SLN

2.4.1. Size and surface charge of SLN

The mean diameter of SLN and polydispersity index, as a measure of dispersion homogeneity (polydispersity index > 0.3 indicates heterogeneity), were estimated using photon correlation spectroscopy (PCS, Zetasizer nano-ZS, Malvern Instrument, UK) at a fixed angle of 173° (other parameters: $T = 25$ °C, repetition 3, λ (He–Ne laser light) 633 nm, diffraction index of medium 1.330). The same instrument was used to measure zeta potential (ZP), which is based on the mobility of charged particles in an electric field. Charge on NPs surfaces strongly influenced the stability of suspended NPs. Particles are unstable when the absolute value of ZP is lower than 5 mV.

2.4.2. Shape and morphology of SLN

Droplets of diluted dispersions of SLN, SLN-D and SLN-C were deposited on freshly cleaved mica sheets and dried for 24 h at room temperature in a Petri dish to protect the sample against dust contamination. Appearance of the SLN was determined by tapping mode imaging performed on an Agilent 5500 Atomic Force Microscope (AFM) (Agilent Technologies, Santa Clara, USA) with a silicone-nitride probes (PPP-FM, Nanosensors, Germany) having nominal force constant 2.8 N/m and resonance frequency 75 kHz. The scan speed was 0.7 lines/s. Scan sizes were taken from 1 μm to 0.3 μm, with 256 × 256 px resolution. Topography, amplitude and phase data were collected simultaneously for all samples. Image analysis was carried out using the Picoview software package (Agilent, USA).

2.4.3. Influence of incorporated 14-DACA and 6-coumarin on SLN structure

The presence of 14-DACA and 6-coumarin in NPs was evaluated by roughness analysis using AFM when NPs' were dispersed in water or methanol. Due to the good solubility of 14-DACA and 6-coumarin in methanol, probes are released from the NPs and, consequently, their surface altered. The calculated roughness values are derived from the Picoview software package. The average roughness (R_a) is defined as the arithmetic mean of deviations in height (Eq. (1)), and the root mean square roughness (R_q), sometimes called the quadratic mean, is the square root of the mean squared value of z values (Eq. (2)).

$$R_a = \frac{1}{n_x n_y} \sum_{i=1}^{n_x} \sum_{j=1}^{n_y} |Z(i,j) - Z_{ave}| \quad (1)$$

where $Z(i,j)$ denotes the topography data for the surface after specimen tilt-correction; Z_{ave} is the average surface height; i and j correspond to pixels in the x and the y direction. The maximum number of pixels in the two directions are given by n_x and n_y.

$$R_q = \sqrt{\frac{\sum (Z_i - Z_{ave})^2}{N}} \quad (2)$$

where Z_{ave} is the average of the z values within the given area; Z_i is the z value for a given point; N is the number of points within the given area.

2.4.4. Thermograms of SLN, SLN-D and SLN-C

The physical state of 14-DACA or 6-coumarin incorporated in SLN was characterized using a differential scanning calorimetric (DSC) thermogram analysis (Mettler Toledo, DSC821). Each sample (probe alone, unlabeled SLN and labeled SLN), approximately 1–3 mg, was sealed separately in a standard aluminum pan and purged in the DSC with pure dry nitrogen set at a flow rate of 50 mL/min. The heating speed was set at 5 °C/min, and the heat flow was recorded from 0 to 100 °C (for 14-DACA, SLN-D) and from 0 to 230 °C (for 6-coumarin, SLN-C and unlabeled SLN).

2.5. Release of 14-DACA and 6-coumarin from labeled SLN

Release profiles of 14-DACA and 6-coumarin from SLN were obtained by the dialysis bag method, with ethanol (63%, v/v) as dialysis medium to ensure sink diffusion conditions. 1 mL samples of dispersions SLN, SLN-D and SLN-C, were placed into pre-swelled dialysis bags with a 12-kDa molecular weight cut-off (Sigma). The bags were immersed into 100 mL of dialysis medium and stirred gently. Samples (300 μL) were removed into 0.5 mL ependorf tubes at defined time intervals. The fluorescence intensity of each sample was measured at the wavelength of emission maximum using an automated plate reader (Tecan, Mannedorf/Zürich, Switzerland). All the operations were carried in triplicate and average results are plotted as a function of time. The amount of 14-DACA or 6-coumarin released from the dialysis bag was expressed according to Eq. (3).

$$\text{Releasing of the probe} = \frac{Fs_t - Fb_t}{Fs_e - Fb_e} \times 100\% \quad (3)$$

where Fs_t and Fb_t are the fluorescence intensities of labeled and unlabeled SLN at time t; Fs_e and Fb_e are the intensities of labeled and unlabeled SLN at the end of dialysis.

2.6. Biological characterization of SLN-D

2.6.1. Cell culture

The immortalized human keratinocyte cell line NCTC2544 (keratinocytes; ICLC, University of Genova, Italy) was used for biological characterization of NPs, due to their culture as adherent monolayers and relatively fast growth that requires routine split 1:4 every 3–4 days. The keratinocytes were grown in Minimum essential medium (MEM) supplemented with 10% (v/v) fetal bovine serum (Gibco®, Invitrogen, USA), 1% (v/v) non-essential amino acids, 2 mM L-glutamine and 100 U/mL antibiotic/antimycotic and maintained at 37 °C in a humidified atmosphere of 5% CO_2 in air.

For examination, the cells were seeded on an appropriate growing area and, after one day (attachment phase), treated with NPs' formulation. Control cultures received only supplemented MEM instead of test dispersions.

2.6.2. Cytotoxicity of SLN with 14-DACA

Cells were treated for 24 h with SLN-D, then trypsinized, centrifuged and diluted appropriately with phosphate buffer (PBS) to obtain cell dispersion.

2.6.2.1. Viability of cells after SLN addition. Viability of cells was determined using propidium iodide (PI, Sigma), a membrane impermeable probe generally excluded from viable cells. After incubating with DNase-free RNase A (100 μg/mL; Applied Biosystems, Foster City, CA, USA) for 30 min, PI (40 μg/mL; Sigma) was added and, after 5 min, PI fluorescence was measured in the FL2 channel of a flow cytometer (FacsCalibur cytometer; BD Biosciences, San Diego, USA). 20,000 gated events were collected for each analysis. The results are present as (i) cells with high fluorescence (dead cells) and (ii) cells with low fluorescence (alive cells) each as a percentage of all evaluated cells.

2.6.2.2. Alterations in cell cycle distribution. Cell cycle distribution of cell dispersion was observed using PI that binds to DNA. Cells (app. 1×10^6) were fixed with ice-cold methanol at −20 °C for 2 h and then resuspended in PBS to give a cell dispersion of 5×10^5 cells/mL. It was incubated with DNase-free RNase A (100 μg/mL; Applied Biosystems, Foster City, CA, USA) for 30 min and PI (40 μg/mL; Sigma) for 15 min at room temperature in the dark. PI fluorescence intensity was quantified in the FL2 channel of flow cytometer (FacsCalibur cytometer; BD Biosciences, San Diego, USA). 20,000 gated events were collected for each analysis. The cell cycle profile, presented as four phases – subG1 (cells with fragmented DNA), G1 (diploid cells with one-chromatid chromatin), S (cells, preparing for division) and G2/M (diploid cells with two-chromatid chromatin) – was analyzed with CellQuest Pro software (BD Biosciences).

2.6.3. Trafficking of SLN in cell culture of keratinocytes

2.6.3.1. Time-lapse internalization. The passage of SLN over the cell-surface, the rates of their internalization and their intracellular movement were monitored by live cell imaging. Cells were plated into sterile glass chamber slides (Lab-tek Nunc, Roskilde, Denmark) and incubated overnight. Immediately after the addition of SLN-D or SLN-C, the time-lapse of blue or green fluorescence intensity was monitored on an Olympus IX81 fluorescence microscope. Transmission micrographs and fluorescence images were collected simultaneously with the same focus settings and merged with Cell® Software (Olympus).

2.6.3.2. Intracellular positioning of SLN. Labeled SLN in the cells were visualized by preparing fixed-slides of treated cells. Keratinocytes were plated on square glass cover slips in 6-well plates. Following 24 h-incubation with SLN-D or SLN-C the cells were fixed (4% paraformaldehyde) and permeabilized (0.1% Triton X-100). Nuclear morphology was visualized using PI (100 μg/mL) (with pre-incubation of DNase-free RNase A) for 5 min in the dark. Actin fibers were stained with green-labeling probe Phalloidin–Fluorescein isothiocyanate (Phalloidin–FITC; Sigma, Chemical Co., Saint Luis, USA) according to the manufacturer's instructions. After staining, the cover slips were removed from the wells, mounted on a slide and viewed using the following excitation/emission filter sets: 360 nm/420 nm (SLN-D), 450 nm/535 nm (Phalloidin–FITC, SLN-C), 535 nm/635 nm (PI). Pictures were observed using the 60-fold objective magnification. Transmission micrographs and fluorescence images were merged or graphs of fluorescence intensity were processed with Cell® Software on an Olympus IX 81 fluorescence microscope.

2.7. Statistical analysis

Data were expressed as means ± S.D. of triplicate analyses and are representative of at least three independent experiments. Differences between samples were evaluated statistically using the unpaired, two-tailed Student's *t*-test. Significance was tested at the 0.05(*) and 0.001(**) levels of probability.

3. Results

3.1. Synthesis and characterization of the new fluorescent probe

14-DACA, 7-(diethylamino)-2-oxo-N-tetradecyl-2H-chromene -3-carboxamide, is an amide formed between 7-diethylaminocoumarin-3 carboxylic acid and 1-aminotetradecane, while in 6-coumarin the benzothiazole is attached on 3rd position of 7-diethylaminocoumarin. Structural formulae and some physical characteristics, like molecular mass, clogP, surface tension, longest molecular dimension, molecular surface electrostatic potential and spectral characteristic of 14-DACA and 6-coumarin are listed in Fig. 2 and Table 1.

The structures of 14-DACA and 6-coumarin are substantially different: 6-coumarin is more globular (longest dimension is 1.67 nm), while 14-DACA is elongated, with the longest dimension equal to 3.08 nm. The lipophilic character of 14-DACA is located predominantly in the aliphatic alkyl chain. Its lipophilicity (clogP) is 4 order of magnitude larger than that of 6-coumarin. We believe that the alkyl chain of 14-DACA makes this molecule more like the components of SLN and therefore it is more easily entrapped into SLN than 6-coumarin. The polar area in each probe is located in the same region (Fig. 2), is practically in the middle of the rigid 6-coumarin molecule. In 14-DACA the molecular electrostatic potential is more pronounced in the same molecular region but the alkyl chain is flexible, which permits adaptation to the SLN interior. In the polar region 6-coumarin can create H-bonds only as proton acceptors while 14-DACA is both – a proton acceptor and a proton donor. The possibility of H-bond formation between the probes and particular components of SLN cannot be deduced from our data, but it is reasonable to expect that the alkyl chain of 14-DACA contributes predominantly to the favorable properties of 14-DACA.

The lipophilic chain in 14-DACA does not significantly change the spectrum of basic coumarin, thus it fluoresces with a bright blue color at ∼470 nm. The presence of the heterocycle in the 6-coumarin shifts the emission to slightly longer wavelength at ∼510 nm, which is in a range of green emitting color (495–570 nm). Furthermore, 14-DACA has a Stokes' shift of 50 nm, while in 6-coumarin it is 40 nm (Fig. 2). The signal isolation of 14-DACA with longer Stokes' shift enables better fluorescence and therefore less interference from Rayleigh-scattered excitation light.

Furthermore, 14-DACA has a lower surface tension than 6-coumarin, which can influence the characteristics of the fluorescently labeled NPs (Table 2, Fig. 3). The different molecular geometry results in different physicochemical properties – the DSC and release profiles for 14-DACA and 6-coumarin both differ.

3.2. Effect of fluorescent probes on SLN properties

The main characteristics of prepared SLN are listed in Table 2. The sizes of SLN and SLN-C are around 200 nm while SLN-D are ∼30% smaller. All sizes are close to those of NPs that are easily internalized into almost all cells.

Diameter and the height of the SLNs obtained by AFM are presented in Table 2. The resulting size diameters obtained by PCS

Table 1
Chemical and physical properties of 14-DACA and 6-coumarin. Surface tension was calculated by ACD/ChemSketch, while all other characteristics were calculated by ChemOffice (CambridgeSoft) software.

Characteristics	14-DACA	6-Coumarin
Molecular formula	$C_{28}H_{44}N_2O_3$	$C_{20}H_{18}N_2O_2S$
Average mass (Da)	456.7	350.4
Partition coefficient	9.28 ± 0.75	6.06 ± 0.75
Surface tension (mN/m)	41.8 ± 3.0	60.8 ± 3.0

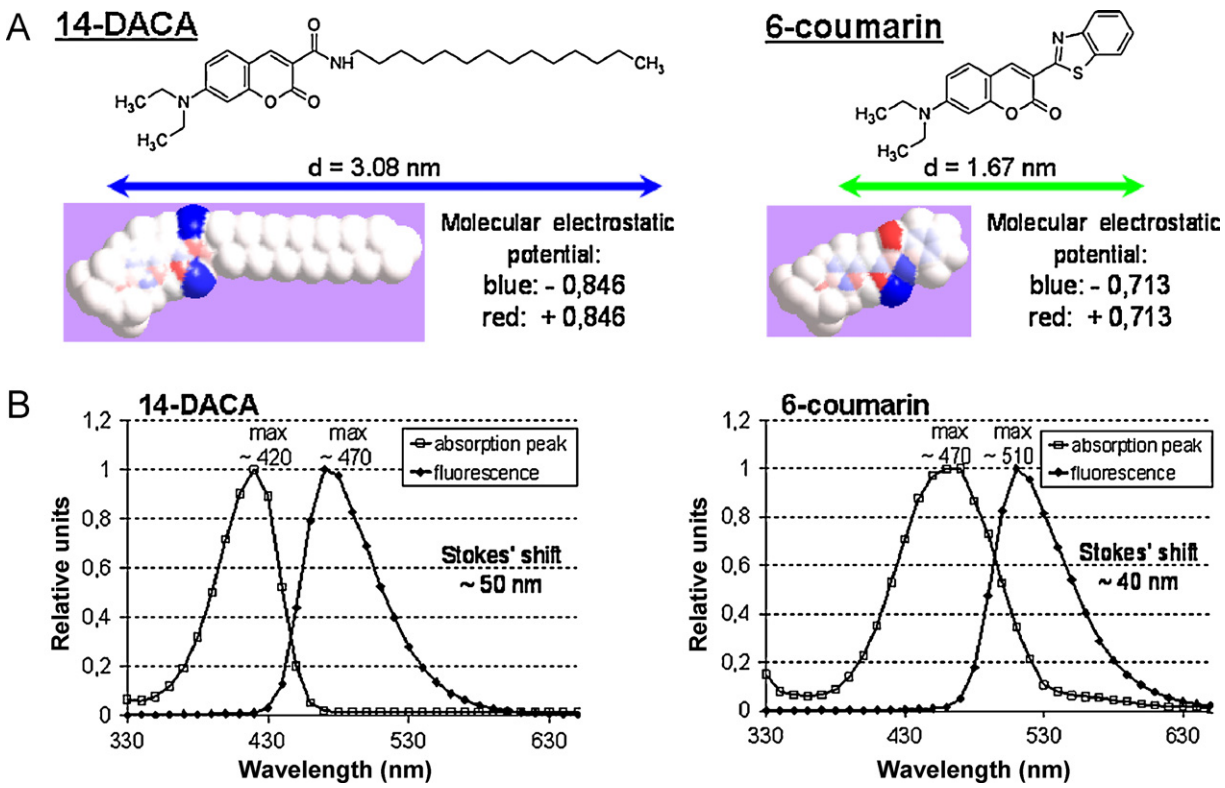

Fig. 2. Chemical properties of 14-DACA and 6-coumarin (A) and their spectra, scanned by automated plate reader (Tecan, Mannedorf/Zürich, Switzerland) (B). Longest molecular dimension and molecular surface electrostatic potential were obtained by ChemOffice (CambridgeSoft) software.

and AFM for SLN and SLN-C are comparable, while for SLN-D are slightly different. PCS is the method based on averaging in order to express size of the particles. On contrary, AFM reveals single particle properties that can deviate from the average. Moreover, the elevated values estimated by AFM can be assigned to the tip sample convolution, which increases the real NPs diameter. The height of all three samples was decreased relative to the width, suggesting a flattening caused by the drying process, which prevented correct measurement of the height. The AFM images confirm that the NPs are flat-circular in shape and with different surface roughness (Fig. 3).

Incorporation of fluorescent probes into the SLNs' structure was confirmed by comparing the roughnesses of NPs' samples dispersed in water and in methanol. In contrast to water, 14-DACA and 6-coumarin are well soluble in methanol, thus their complete release out from SLN is expected. Eventually, in the case of labeled SLN (SLN-D and SLN-C) the roughness dropped almost to the level of the control (SLN) (Table 3).

Additionally, the presence of fluorescent probes in NP structure was also monitored by DSC. From DSC results, it was observed that the endothermic peak of lipid component, with onset at around 72 °C, is slightly changed and moved when the fluorescent probes are present (Fig. 4). Associated thermograms of unlabeled SLN and free fluorescent probes (14-DACA or 6-coumarin) were observed when DSC analysis was done for a mixture of unlabeled SLN and 14-DACA or unlabeled SLN and 6-coumarin (data not shown). The endothermic peak of 14-DACA was found at ~75 °C (an onset at 77.87 °C) and of 6-coumarin at ~210 °C (an onset at 208.67 °C). These characteristic peaks were not observed in SLN labeled with 14-DACA (SLN-D) and 6-coumarin (SLN-C). The absence of detectable crystalline domains of fluorescent probes in SLN clearly indicates that molecules of 14-DACA and 6-coumarin are in the amorphous or in the solid-state solubilized form in the solid lipid matrix. This state of the probe inside the matrix enables sustained release of the probe from the NPs.

Release profiles of probes from loaded SLN are presented in Fig. 5, where the chemical properties of the investigated probes are manifested. 14-DACA from SLN-D is released significantly slower than of 6-coumarin from SLN-C in the first 8 h. The release profile of 6-coumarin shows a biphasic pattern: a rapid initial release, in 4 h 80%, followed by a slower release, while the release of 14-DACA from SLN-D is practically linear in the 8 h.

3.3. Cytotoxicity of SLN-D

The influence of SLN-D on the cells was investigated because recognition of a harmful effect of fluorescent probes can discard their usage in biological investigations. It is known from the literature that SLN and SLN-C are not cytotoxic (Kristl et al., 2008; Teskac and Kristl, 2010). The effects of SLN-D on via-

Table 2
Physical characteristics of SLN, SLN-D and SLN-C, determined by PCS (Photon Correlation Spectroscopy) and AFM (Atomic Force Microscopy).

Characteristics	Method	SLN	SLN-D	SLN-C
Size (nm)	PCS	181.6 ± 1.6	122.8 ± 10.5	195.0 ± 12.8
Polydispersity index	PCS	0.452 ± 0.004	0.232 ± 0.008	0.371 ± 0.046
Zeta potential (mV)	PCS	−18.5 ± 0.4	−20.4 ± 0.5	−21.9 ± 0.6
Width (nm)	AFM	231.0 ± 53.0	250.8 ± 21.7	182.4 ± 14.3
Height (nm)	AFM	10.7 ± 2.3	14.1 ± 2.3	7.4 ± 0.7

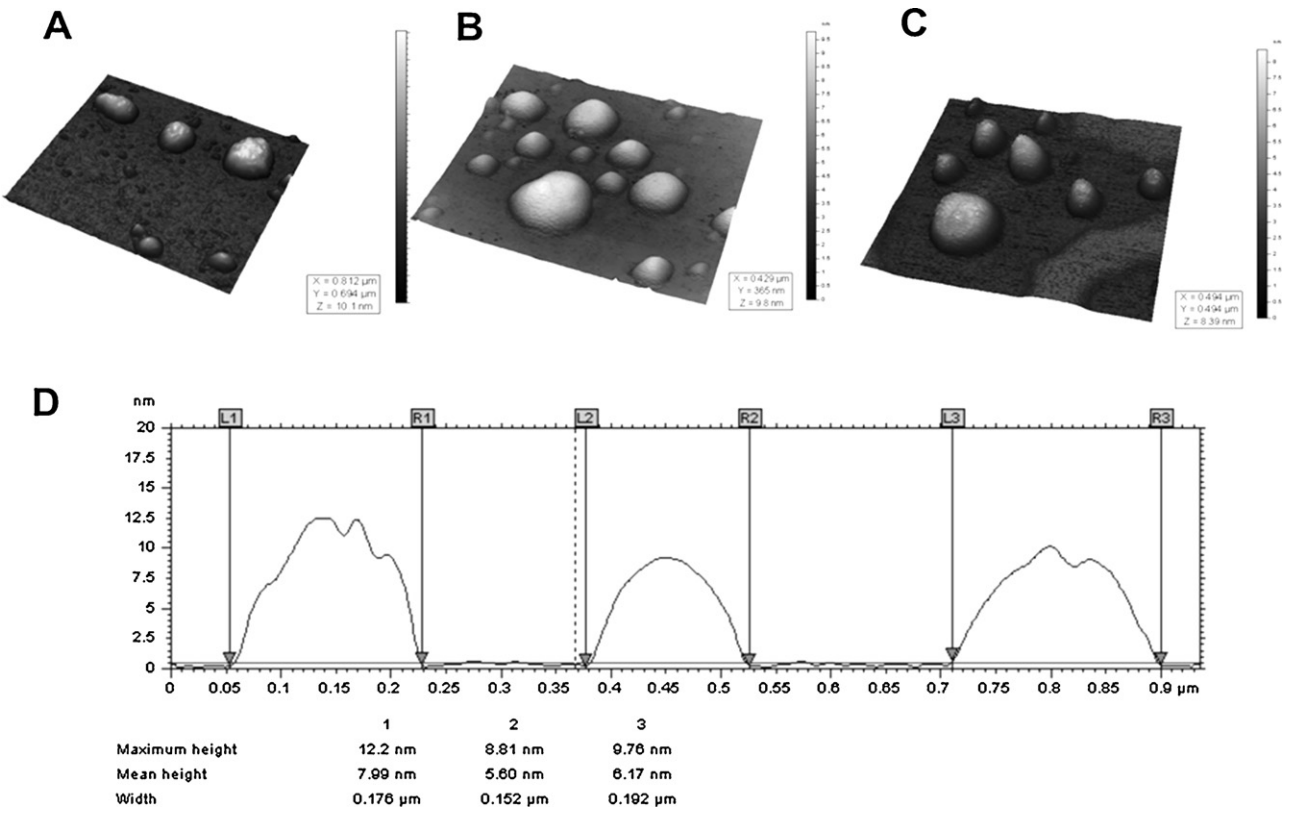

Fig. 3. AFM images (tapping mode) of unlabeled SLN (A), SLN labeled with 14-DACA (B) and labeled with 6-coumarin (C), diameter and height of nanoparticles (D).

Table 3
Roughness data of the investigated SLN dispersed in water and methanol. Roughness parameters (R_a and R_q) have been determined along the profile of individual particles. Values are expressed in nanometers.

Dispersing media	SLN		SLN-D		SLN-C	
	R_a	R_q	R_a	R_q	R_a	R_q
Water	0.2 ± 0.01	0.3 ± 0.05	3.7 ± 0.9	3.7 ± 0.5	2.1 ± 0.50	2.8 ± 0.6
Methanol	0.2 ± 0.01	0.3 ± 0.05	0.4 ± 0.13	0.5 ± 0.2	0.3 ± 0.10	0.4 ± 0.10

bility and cell cycle distribution are shown in Fig. 6. Results clearly demonstrate that the presence of 14-DACA in SLN caused neither cytotoxicity nor influenced particular phases in cell cycle.

3.4. SLN uptake kinetics and intracellular localization

The cellular uptake processes of SLN were recorded by fluorescence microscopy, using time-lapse imaging, with associated computational analysis. Both 14-DACA and 6-coumarin demonstrated effective cellular internalization of SLN, as seen by increasing of blue fluorescence with time for SLN-D and green fluorescence for SLN-C (Figs. 7 and 8). SLN-D are still seen inside the cells as separate blue dots after 90 min, while SLN-C is releasing 6-coumarin (green color) after 45 min and the green fluorescence is spread over the intracellular space (Fig. 7).

The images (Figs. 7 and 8) reflect the position of labeled SLNs as a function of time. While the presence of individual SLN-D particles inside the cells is clearly seen as separate dots of blue fluorescence, the SLN-C particles are not sharply shown. These results are confirmed by the profiles of relative fluorescence intensity in the cell cross section shown on Fig. 9. Fluorescence intensity of SLN-C is spread broadly over the cell interior. Contrary, the precise location of SLN-D inside the cells is better defined. Each SLN-D is shown by a sharp peak in a profile of fluorescence intensity. Interestingly, in both cases, the fluorescence intensity of the SLNs decreases in

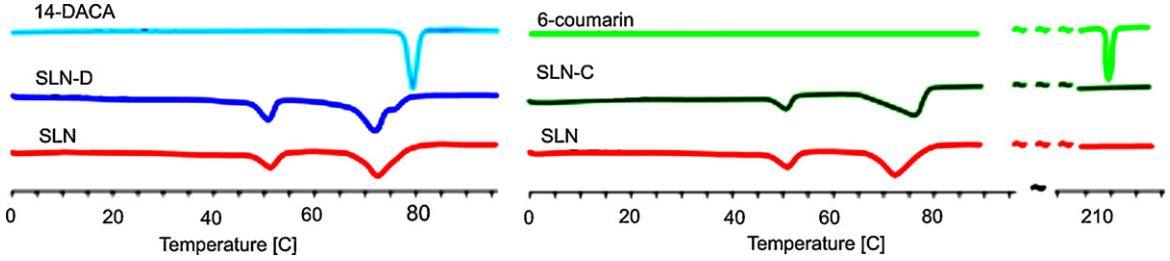

Fig. 4. DSC thermograms of SLN, 14-DACA, 6-coumarin, SLN-D, and SLN labeled with 6-coumarin (SLN-C).

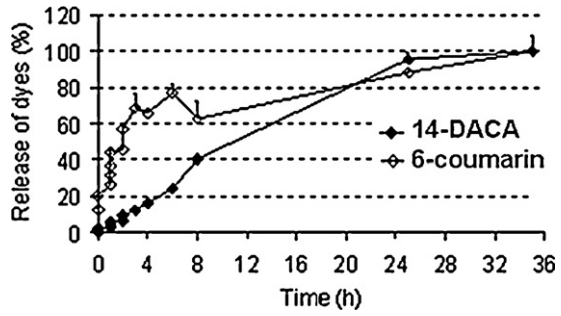

Fig. 5. Release profiles of 14-DACA from SLN-D and 6-coumarin from SLN-C. To maintain steady state due very low solubility of the probes in water the dialysis medium for both probes was 63 (v/v) % ethanol.

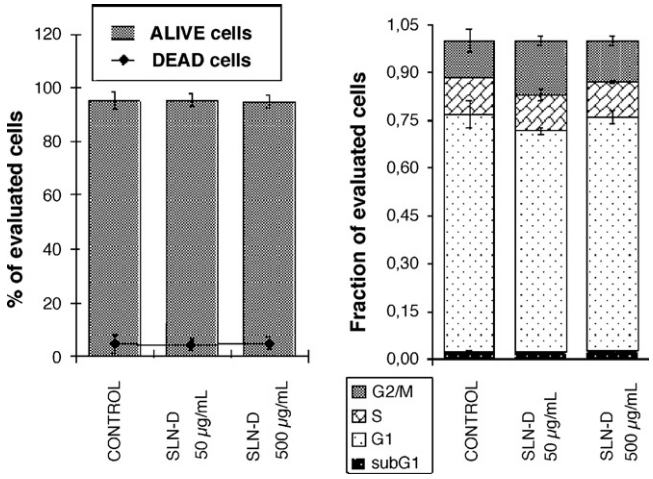

Fig. 6. Viability (left) and cell cycle distribution (right) of cells. 2×10^5 keratinocytes were treated with 50 μg/mL or 500 μg/mL of SLN-D for 24 h and finally analyzed on the FL2 channel of flow cytometer.

the area of red fluorescence that indicates nucleus. This proves the localization of SLNs outside the nucleus.

3.5. 14-DACA enables precise multicolor imaging

The realization of multicoloring experiments using 14-DACA labeled SLNs is demonstrated in Figs. 9 and 10. The emission spectra of fluorescent compounds appropriate for analytical studies should be separated sufficiently from their excitation spectra to ensure good signal isolation. The presence of components in solution that absorb light at or near the excitation wavelength of the fluorophore cause decreased fluorophore fluorescence.

The nuclei of keratinocytes treated with SLN-C and stained with red emitting propidium iodide (PI), are seen as yellow, because the emission spectrum of 6-coumarin is covered with the excitation spectrum of PI (Figs. 8 and 9). This hinders the determination of the exact localization of SLN-C inside the cell. Contrary, there is no interference of 14-DACA with PI and therefore the nucleus is colored red, as expected. Fig. 10 shows the most promising example of the multicoloring approach to visualize the exact location of SLN inside keratinocytes. The positions of SLN-D (blue dots in Fig. 10) are very well distinguished from the red nucleus (PI) and green actin fibers. The multilabeling approach is much more informative with 14-DACA than with 6-coumarin.

4. Discussion

For particular purpose, e.g. to follow nanosized drug carriers, a proper fluorescent probe has to be carefully selected. We have designed and prepared a novel fluorescent probe, 14-DACA, with coupling of coumarin derivatives with tetradecyl amine.

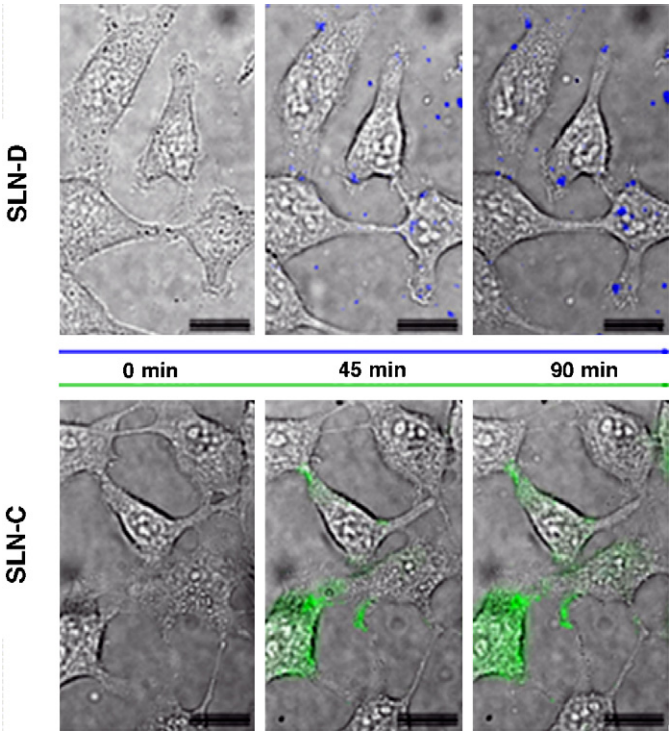

Fig. 7. Internalization of SLN-D (blue) and SLN-C (green) in a culture of keratinocytes. Dispersions of SLN-D or SLN-C were added to the cells and their movement followed by time-lapse fluorescence microscopy (Olympus IX 81). The images are merged transmission and fluorescence micrographs. Legend: blue – SLN-D; green – SLN-C. Bar is 20 μm.

4.1. Comparison of 14-DACA and 6-coumarin in SLN

We successfully characterized SLNs labeled with the investigated probes. AFM and DCS measurements as well as dissolution test confirmed incorporation of the both, 14-DACA and 6-coumarin, into the matrix of SLNs. Incorporation of the 14-DACA was indirectly confirmed by AFM using surface roughness analysis too. We found that the presence of 14-DACA reduces the size of SLNs and the polydispersity index become smaller as well. The difference in the sizes (Table 2) between the samples (SLN, SLN-D, SLN-C) is ascribed to the presence of fluorescent probes. 14-DACA acts as a non-ionogenic surface active compound (see surface tension Table 1), and it can enhance the contact between melted lipids and aqueous phase, which enables the formation of smaller droplets and consequently NPs. This effect is already described in the literature and is related to insufficient concentration of surfactant in NPs that induced polymorphic transitions of lipids in a core and consequently changing the shape and size of NPs (Helgason et al., 2009). On the other hand, the surface tension of 6-coumarin is higher than that of 14-DACA and decreases interfacial tension less than 14-DACA. Therefore, the size of SLN-C does not differ significantly from unlabeled SLN. The polydispersity index of SLN dispersions are widespread, ranging from approx. 0.23 for SLN-D to 0.37 for SLN-C and 0.45 for SLN, pointing on the presence of NPs with different sizes, seen also on the AFM images (Fig. 3). Wider size distribution of SLN and SLN-C is attributed to the absence of additional molecules, which can act as a surfactant, such as 14-DACA. "Uncovered" surface of NPs results in increased attractive interaction between NPs and caused aggregation and increased the polydispersity index. However, the zeta potentials of the dispersions are around −20 mV,

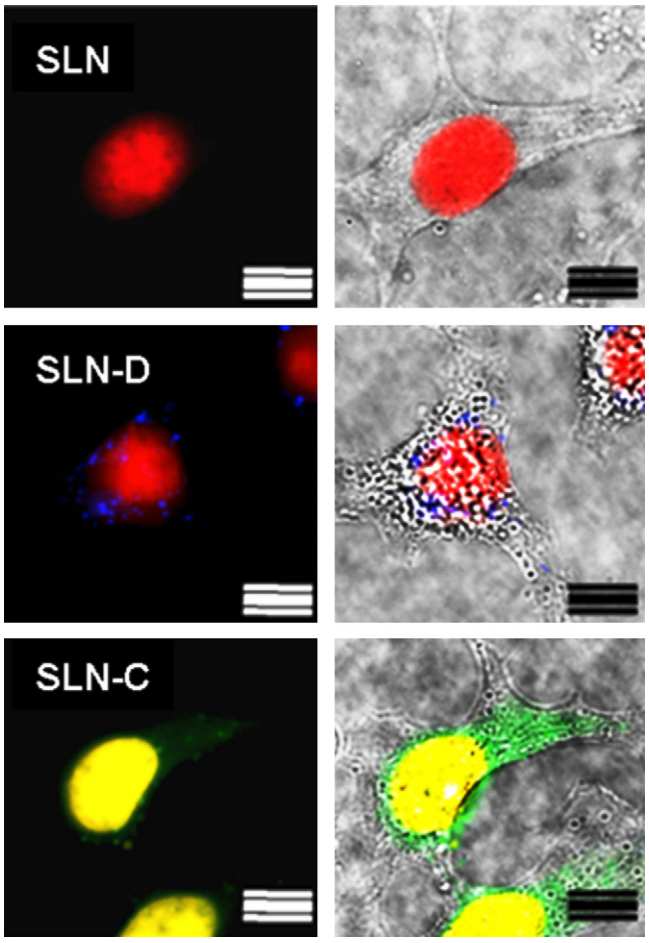

Fig. 8. Multicolor imaging of intracellular localization of SLN. Keratinocytes were incubated with SLN-D or SLN-C for 24 h and fixed-slides then prepared. Images (right) were recorded using a fluorescence microscope (Olympus IX 81) by merging transmission micrographs and fluorescence images (left). Legend: red–nuclei stained with propidium iodide; blue - SLN-D; green - SLN-C. Bar is 20 μm.

which enable the mutual repulsion of the NPs and prolong their half life.

Positioning of fluorescent dyes, 14-DACA and 6-coumarin, into NPs' structure was proved by AFM technique (Table 3) and DSC

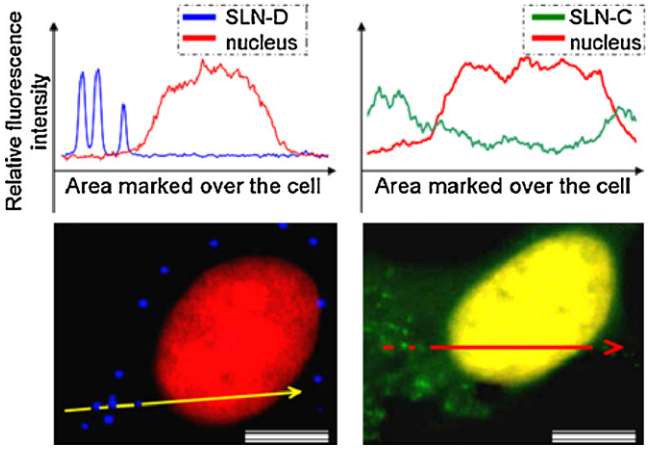

Fig. 9. Differences in the brightness and distinctness of labeled SLN (SLN-D and SLN-C) incubated in cell culture. Graphs represent relative fluorescence intensity of nanoparticles and nuclei regarding the arrow marked on the fluorescence picture below. Images and graphs were made using CellR̂ Software on a fluorescence microscope (Olympus IX 81). Bar is 10 μm.

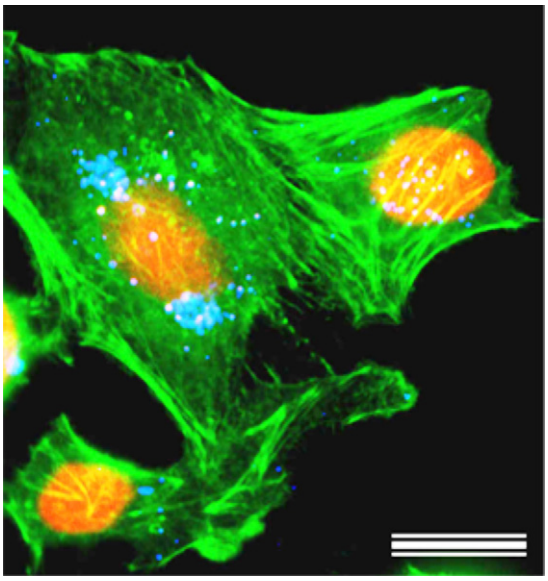

Fig. 10. Multicolor imaging and intracellular localization of fluorescently labeled nanoparticles. Keratinocytes were incubated with SLN-D or SLN-C for 24 h. Fixed-slides were prepared and imaged by fluorescence microscope. Legend: red–nuclei stained with propidium iodide; blue – SLN-D; green – actin, stained with phalloidin-FITC. Bar is 20 μm.

analysis (Fig. 4). By using AFM the effect of the fluorescent probe on the surface roughness of SLN was established by roughness analysis of individual particles (Table 3). When SLN-C or SLN-D were dispersed in aqueous media, the roughness parameters (R_a, R_q) were significantly higher in comparison to the R_a or R_q of unlabeled SLN. However, surface roughness parameters of SLN-D and SLN-C after dispersing in methanol showed values comparable to those of SLN. Methanol triggered release of fluorescent probes from the NPs' structure, confirming that fluorescent probes are loaded into SLNs' structure and influenced on NPs' surface properties. Preliminary results obtained by AFM should be additionally confirmed by others complementary techniques on single particles involving surface chemical mapping. Next, DSC results clearly indicate that fluorescent probes, 14-DACA and 6-coumarin, exist in the solid lipid matrix of SLN as an amorphous or solid-state solubilized form (Fig. 4). Furthermore, dialysis method showed more strongly incorporation of 14-DACA into SLN structure in comparison with 6-coumarin, which is positioned closer to the NPs' shell (Fig. 5).

4.2. Influence of 14-DACA on cell viability

Cells treated with SLN-D up to concentration of 500 μg/mL in a culture of 2×10^5 keratinocytes did not differ significantly in viability and cell cycle distribution from control cells (Fig. 6). Treated cells were well spread over the cell growing area without any observed alterations, such as intercellular disconnections or detachment (data not shown). Particular phases of cell cycle distribution of cells treated with 50 or 500 μg/mL of SLN-D did not differ significantly from that of the control. Therefore, our cytotoxic study on cells confirmed non-cytotoxic effect of 14-DACA on keratinocytes what is in accordance with the literature data (Farazi et al., 2001). Tetradecyl alkyl residue into new coumarin fluorescent probe keeps biological similarity with its function as anchor for lipoproteins into biological membranes. Currently available reports about new fluorescent probes are mostly oriented on cyclic structural and physicochemical properties, labeling technology and application, but biocompatibility or toxicity data are frequently missing (Gonçalves, 2009; Maier et al., 2002). Finally, Fei and Gu (2009) have reported that fluorescent dye conjugated

with chitosan can obviously increase the degree of biocompatibility and decrease the degree of toxicity.

4.3. SLN uptake and intracellular localization

Following the uptake of SLN and their trafficking in the cells are imperative to fully explore their usage as efficient intracellular drug delivery system for the range of therapeutic targets, which could be located in the cytosol or at a deeper level within intracellular organelles. It is known that SLN crosses the keratinocytes' membrane in less than a minute (Teskac and Kristl, 2010). Initially, the SLN were located on the periphery, but quickly moved towards the perinuclear region and do not stay in one flat surface. To resolve certain cellular organelles (like the nucleus, endoplasmic reticulum, mitochondria, etc.) and track proteins or other biomolecules in live cells, numerous fluorescent dyes are available (Fernández-Suárez and Ting, 2008; Spandl et al., 2009). On the other hand, there are lack of fluorescent dyes and probes for particular drug nanocarriers. Inorganic or fluorescent polystyrene NPs are generally used as model particles for fluorescence microscopy and obtained pictures of their presence in cell culture are bright and location of NPs in cellular compartments can be precisely determined (Oh et al., 2006). However, these NPs may not be suitable alternatives to biodegradable and biocompatible nanosized particles loaded with drug molecules (e.g. SLN, polymeric NPs) for fluorescence microscopy studies mainly because they do not contain therapeutic agent and because of the differences in their physical properties, including hydrophobicity, surface charge, particle size distribution, different density and protein adsorption, etc.

Disadvantage of most frequently used 6-coumarin for staining drug nanocarriers is its leakage and self-quenching. Additionally, when SLN-C is present in the cell culture, particles were hardly to extract from extensive green background (Figs. 7–9). However, similar to our case, self-quenching of 6-coumarin was already shown by some other researchers too, e.g. Panyam and Labhasetwar (2003). At least, staining the NPs by 14-DACA enabled excellent multicoloring, where great positioning of NPs, separate from cellular compartments, was obtained. This result shows an excellent progress on the area of drug delivery systems and proofs that using case-designed fluorescent probe for particular nanosized system enables distinct and undoubting visualization in the intracellular environment what can be beneficial upgrade to the current nanoscience.

5. Conclusion

The results of our study provide important information regarding localization of nanoparticulate carriers in the cells as well as their intracellular fate if 14-DACA probe was used. Probe' spectra do not cover each other, contributing to effective distinguishing between the labeled cellular compartments and fluorescent nanosized carriers. New synthesized fluorescent probe 14-DACA is not cytotoxic, has high lipophilicity and good anchoring into SLN. 14-DACA gives bright fluorescence pictures in cellular environment, where lipids NPs are seen distinctly as blue dots. Moreover, spectra of 14-DACA are well distinguished from spectra of another fluorescent probe, what enable clear multicolor imaging. We can conclude that 14-DACA provides an accurate repertoire of drug uptake and can be a powerful tool to produce precise, quantitative data in real time that is required for the elucidation of the complex process at intracellular drug delivery and distribution.

Acknowledgements

The authors thank Faculty of Chemistry and Chemical Technology, University of Ljubljana, for CHN analysis and Institute Josef Stefan for MS analysis. We also acknowledge Prof. Roger H. Pain for proof reading the manuscript. This work was supported by the Slovenian Research Agency grants: P1-0189, P1-0208 and 312243-1/2007.

References

Ahlin, P., Kristl, J., Smid-Korbar, J., 1998. Optimization of procedure parameters and physical stability of solid lipid nanoparticles in dispersions. Acta Pharm. 48, 259–267.
Biswas, S., Dodwadkar, N.S., Sawant, R.R., Koshkaryev, A., Torchilin, V.P., 2011. Surface modification of liposomes with rhodamine-123-conjugated polymer results in enhanced mitochondrial targeting. J Drug Target., doi:10.3109/1061186X. 2010.536983.
Caddeo, C., Teskac, K., Sinico, C., Kristl, J., 2008. Effect of resveratrol incorporated in liposomes on proliferation and UV-B protection of cells. Int. J. Pharm. 363, 183–191.
Cavalli, R., Donalisio, M., Civra, A., Ferruti, P., Ranucci, E., Trotta, F., Lembo, D., 2009. Enhanced antiviral activity of Acyclovir loaded into β-cyclodextrin-poly(4-acryloylmorpholine) conjugate nanoparticles. J. Control. Release 137, 116–122.
Cu, Y., Saltzman, W.M., 2009. Controlled surface modification with poly(ethylene)glycol enhances diffusion of PLGA nanoparticles in human cervical mucus. Mol. Pharmacol. 6, 173–181.
Farazi, T.A., Waksman, G., Gordon, J.I., 2001. The biology and enzymology of protein NMyristoylation. J. Biol. Chem. 276, 39501–39504.
Fei, X., Gu, Y., 2009. Progress in modifications and applications of fluorescent dye probe. Prog. Nat. Sci. 19, 1–7.
Fernández-Suárez, M., Ting, A.Y., 2008. Fluorescent probes for superresolution imaging in living cells. Nat. Rev. Mol. Cell Biol. 9, 929–943.
Gillmeister, M.P., Betenbaugh, M.J., Fishman, P.S., 2011. Cellular trafficking and photochemical internalization of cell penetrating peptide linked cargo proteins: a dual fluorescent labeling study. Bioconjug. Chem. 22, 556–566.
Gonçalves, M.S., 2009. Fluorescent labeling of biomolecules with organic probes. Chem. Rev. 109, 190–212.
Harush-Frenkel, O., Debotton, N., Benita, S., Altschuler, Y., 2007. Targeting of nanoparticles to the clathrin-mediated endocytic pathway. Biochem. Biophys. Res. Commun. 353, 26–32.
Hearnden, V., Lomas, H., Macneil, S., Thornhill, M., Murdoch, C., Lewis, A., Madsen, J., Blanazs, A., Armes, S., Battaglia, G., 2009. Diffusion studies of nanometer polymersomes across tissue engineered human oral mucosa. Pharm. Res. 26, 1718–1728.
Helgason, T., Awad, T.S., Kristbergsson, K., McClements, D.J., Weiss, J., 2009. Effects of surfactant surface coverage on formation of solid lipid nanoparticles (SLN). J. Colloid Interface Sci. 334, 75–81.
Hironaka, K., Inokuchi, Y., Tozuka, Y., Shimazawa, M., Hara, H., Takeuchi, H., 2009. Design and evaluation of a liposomal delivery system targeting the posterior segment of the eye. J. Control. Release 136, 247–253.
Kristl, J., Teskac, K., Caddeo, C., Abramović, Z., Sentjurc, M., 2009. Improvements of cellular stress response on resveratrol in liposomes. Eur. J. Pharm. Biopharm. 73, 253–259.
Kristl, J., Teskac, K., Milek, M., Mlinaric-Rascan, I., 2008. Surface active stabilizer Tyloxapol in nanoparticle dispersions exerts cytostatic effects and apoptotic dismissal of cells. Toxicol. Appl. Pharmacol. 232, 218–225.
Maier, O., Oberle, V., Hoekstra, D., 2002. Fluorescent lipid probes: some properties and applications. Chem. Phys. Lipids 116, 3–18 (a review).
Miglietta, A., Cavalli, R., Bocca, C., Gabriel, L., Gasco, M.R., 2000. Cellular uptake and cytotoxicity of solid lipid nanospheres (SLN) incorporating doxorubicin or paclitaxel. Int. J. Pharm. 210, 61–67.
Müller, R.H., Mäder, K., Gohla, S., 2000. Solid lipid nanoparticles (SLN) for controlled drug delivery – a review of the state of the art. Eur. J. Pharm. Biopharm. 50, 161–177.
Oh, J.M., Choi, S.J., Kim, S.T., Choy, J., 2006. Cellular uptake mechanism of an inorganic nanovehicle and its drug conjugates: enhanced efficacy due to clathrin-mediated endocytosis. Bioconjug. Chem. 17, 1411–1417.
Pajk, S., Pečar, S., 2009. Synthesis of novel amphiphilic spin probes with the paramagnetic doxyl group in the polar region. Tetrahedron 65, 659–665.
Panyam, J., Labhasetwar, V., 2003. Dynamics of endocytosis and exocytosis of poly(D,L-Lactide-coglycolide) nanoparticles in vascular smooth muscle cells. Pharm. Res. 20, 212–220.
Panyam, J., Sahoo, S.K., Prabha, S., Bargar, T., Labhasetwar, V., 2003. Fluorescence and electron microscopy probes for cellular and tissue uptake of poly(D,L-lactide-co-glycolide) nanoparticles. Int. J. Pharm. 262, 1–11.
Robert, S., Bertolla, C., Masereel, B., Dogne, J.M., Pochet, L., 2008. Novel 3-carboxamide-coumarins as potent and selective FXIIa inhibitors. J. Med. Chem. 51, 3077–3080.
Sharma, P., Brown, S., Walter, G., Santra, S., Moudgil, B., 2006. Nanoparticles for bioimaging. Adv. Colloid. Interface Sci. 123–126, 471–485.
Spandl, J., White1, D.J., Peychl1, J., Thiele, C., 2009. Live cell multicolor imaging of lipid droplets with a new dye, LD540. Traffic 10, 1579–1584.
Teskac, K., Kristl, J., 2010. The evidence for solid lipid nanoparticles mediated cell uptake of resveratrol. Int. J. Pharm. 390, 61–69.
Torchilin, V.P., 2005. Fluorescence microscopy to follow the targeting of liposomes and micelles to cells and their intracellular fate. Adv. Drug Deliv. Rev. 57, 95–109.

Trapani, A., Sitterberg, J., Bakowsky, U., Kissel, T., 2009. The potential of glycol chitosan nanoparticles as carrier for low water soluble drugs. Int. J. Pharm. 375, 97–106.
Watson, P., Jones, A.T., Stephens, D.J., 2005. Intracellular trafficking pathways and drug delivery: fluorescence imaging of living and fixed cells. Adv. Drug Deliv. Rev. 57, 43–61.
White, N.S., Errington, J.R., 2005. Fluorescence techniques for drug delivery research: theory and practice. Adv. Drug Deliv. Rev. 57, 17–42.
Wu, C., Zheng, Y., Szymanski, C., McNeill, J., 2008. Energy transfer in a nanoscale multichromophoric system: fluorescent dye-doped conjugated polymer nanoparticles. J. Phys. Chem. C Nanomater. Interfaces 112, 1772–1781.